Mapping ethylene and acetylene plumes using satellite high-resolution imaging spectrometers that exploit the SWIR spectrum

Javier Roger[1,2*], Adriana Valverde[1], Javier Gorroño[1], Michael Hilker[2], Zhipeng Pei[3], Itziar Irakulis-Loitxate[1], Luis Guanter[1,4]

[1] *Research Institute of Water and Environmental Engineering (IIAMA), Universitat Politècnica de València (UPV), Valencia, Spain.*
[2] *Institute of Environmental Physics (IUP), University of Bremen, Bremen, Germany.*
[3] *School of Remote Sensing and Information Engineering, Wuhan University, Wuhan, China.*
[4] *Environmental Defense Fund, Amsterdam, the Netherlands.*

[*] Now at Institute of Environmental Physics (IUP), University of Bremen, Bremen, Germany.
[*] To whom correspondence should be addressed; E-mail: jroger@iup.physik.uni-bremen.de

Ethylene (C_2H_4) and acetylene (C_2H_2) are reactive hydrocarbons that degrade air quality through ozone formation and atmospheric oxidation. However, space-based monitoring of plumes from these gases remains largely unexplored. Here, we demonstrate, for the first time, that ethylene and acetylene point-source emissions can be detected and quantified using shortwave infrared (SWIR) imaging spectroscopy, overcoming the spatial and spectral limitations of existing thermal infrared observations. As a proof of concept, we apply a matched filter approach to EMIT data to characterize plumes from these gases. We identify two ethylene plumes from industrial facilities in Saudi Arabia and Iraq, and two acetylene plumes from industrial regions in China (Wuhai and Baotou). The retrieved emission rates are consistent with available satellite-based estimates and reveal both previously identified and unreported hotspots, highlighting the potential of SWIR imaging spectrometers for high-resolution monitoring of point-source emissions from these species.

Introduction

Ethylene (C_2H_4) is a volatile organic compound that contributes to air pollution as a precursor of tropospheric ozone and formaldehyde, which ultimately has an impact on human health[1]. It is emitted into the atmosphere from biomass burning, urban activity, and industrial processes, and its production is expected to increase[2].

Franco et al.[3] used satellite-based thermal infrared (TIR) measurements from the IASI instrument[4] and identified over 300 ethylene anthropogenic hotspots. Most of these emissions originated from industry, primarily from the metallurgy, coal, and chemical sec-

tors. Bottom-up emission inventories largely underestimate industrial emissions, and in some cases do not include them. These findings highlight the limitations of current inventories and underscore the importance of space-based emission monitoring for supporting effective environmental policies. Even though IASI could identify and quantify all these hotspots, its coarse spatial resolution ($>$ 12 km) is not sufficient to attribute emissions to their corresponding point sources in large industrial hubs. Instruments with finer spatial resolution are required for this task.

Acetylene (C_2H_2) is another important atmospheric hydrocarbon and a precursor of secondary organic aerosols. It is emitted from biomass burning, biofuel and fossil fuel combustion, and a variety of industrial processes. Using IASI observations, Franco et al.[5] identified 16 anthropogenic acetylene hotspots, all associated with the industrial sector. These hotspots were exclusively located in China, reflecting the country's dominant role in global acetylene consumption[6]. Similar to ethylene, industrial acetylene emissions are likely to be underestimated in current bottom-up emission inventories. However, the relatively weak thermal infrared absorption of acetylene and the coarse spatial resolution limit the accurate quantification of individual point sources from IASI observations.

While ethylene absorption lines in the TIR spectrum are available in public databases, measurements of its absorption in the shortwave infrared (SWIR) are only reported in the literature[7]. From Sharpe et al.[8], we obtained the ethylene cross section spectrum in the 1550–2500 nm spectral range. On the other hand, the acetylene line-by-line absorption spectrum in the SWIR could be found in HITRAN 2024 database[9]. Figure 1 shows the absorption cross sections of ethylene and acetylene together with other important gases within this spectral range. These two gases exhibit absorption features of comparable magnitude to other species that have already been characterized using remote sensing in this region of the spectrum. Several satellite imaging spectrometers provide coverage of the SWIR at relatively high spatial resolution, including EMIT[10], which has a 60 m pixel size. Since methane (CH_4), carbon dioxide (CO_2), and ammonia (NH_3) plumes can be detected with this instrument[11–13], the detection of ethylene and acetylene plumes may also be feasible, potentially improving the characterization of point source emissions in reference to satellite-based TIR measurements.

[Figure 1 about here.]

In this study, we combine ethylene absorption cross sections from Sharpe et al.[8] and acetylene line-by-line absorption data from HITRAN 2024 with EMIT observations to assess the feasibility of detecting and quantifying point-source emissions of these species from space. To demonstrate this capability, we characterize two ethylene plumes originating from industrial areas in Iraq and Saudi Arabia, and two acetylene plumes originating from industrial regions in China (Wuhai and Baotou).

Methods and materials

We acquired L1 data from the EMIT instrument, which are publicly available through the mission data portal. The matched filter method[14] was then applied to derive concentration-path-length enhancement (α) maps of ethylene and acetylene, expressed in ppm·m. These maps were subsequently used to identify and quantify point-source emissions.

Following Roger et al.,[15], multiple iterations and supervised radiance thresholding were added to the basic matched filter implementation. The unit gas absorption spectra (K) of ethylene and acetylene, which is required by this methodology, were derived from high-resolution radiance spectra (0.1 nm). Optical depth spectra were first computed using the HITRAN 2024 line-by-line database and the ARTS radiative transfer model[16], and subsequently converted into radiance spectra using libRadtran[17]. Note that, since ethylene absorption spectra could not be found in the SWIR spectral range in the HITRAN 2024 database, we used the cross section spectrum from Sharpe et al.[8]. This was incorporated into the atmospheric optical depth generated by ARTS. Next, a sea-level surface elevation and a midlatitude summer atmospheric profile from the RFM model[18] were assumed. Several radiance spectra were then simulated for different values of α for ethylene and acetylene. For simplicity, an infinite lifetime for both gases was assumed, and the same α values used for ammonia in Roger et al.,[15] were adopted. The K spectrum was generated following Foote et al.,[19], already accounting for the convolution to the instrument spectral response function and the specific acquisition geometry. We used the 2000–2450 nm spectral range to characterize ethylene and the 1450–1600 nm range for ethylene, as they contain the strongest absorption features of these gases in the SWIR. In addition, K spectra for CH_4, NH_3, CO_2, and water vapor (H_2O) were generated using the same setup as in Roger et al.[15], to enable assessment of potential false positives through comparison with retrievals of other gases.

Atmospheric ethylene and acetylene concentrations were set to zero, as ambient concentrations are typically negligible[20,21]. Furthermore, emissions were assumed to be in the first 500 m above the surface within our reference atmosphere, where a pressure of P = 1 atm and a temperature of T = 294 K were assumed. However, the ethylene cross section spectrum from Sharpe et al.[8] was measured under conditions of P = 1 atm and T = 298.1 K. To assess the impact of this temperature difference, we performed a test using methane as a reference gas. Methane cross section spectra were generated with the HAPI tool[22] using P = 1 atm and temperatures of T = 294 K and T = 298.1 K. Following the procedure described above, the corresponding K spectra for the methane case were generated and compared, revealing no significant changes due to this difference in temperature. A similar behavior is therefore expected for ethylene, indicating that the resulting K spectrum is sufficiently accurate for the consistent detection and quantification of ethylene plumes.

Ethylene and acetylene plumes are quantified using the IME method[23,24], which provides the emission rate (Q) in t h^{-1}. This methodology requires the effective wind speed (U_{eff}), an empirical parameter that relates Q to the mass and spatial extent of the plume. U_{eff} was obtained using a calibration approach similar to that of Guanter et al.,[25], based on the WRF-LES simulations presented by Gorroño et al.[26] and located in Zenodo[27]. This calibration was adapted to the specific molar mass of the gas and to the EMIT instrument by considering the typical noise levels of the retrievals. The lower and upper bounds of the noise range were derived from the same regions used by Roger et al.,[15] for NH_3, and the same emission-rate range was adopted. The resulting calibration is $U_{eff} = 0.48 \cdot U_{10} + 0.59$ for ethylene and $U_{eff} = 0.47 \cdot U_{10} + 0.68$ for acetylene, where U_{10} is the wind speed at 10 m above the surface, obtained from the GEOS-FP product[28]. Note that emission rate uncertainty is calculated as in Roger et al.,[29].

Results and discussion

In the top panels from Figure 2, we show ethylene plumes originating from two different sources. One of these emissions (top left) is located in Yanbu, Saudi Arabia, and is associated with a single source. This source is part of an ethylene hotspot identified by Franco et al.,[3] as a large petrochemical hub. The higher spatial resolution of EMIT allows us to better constrain the potential emission sources to a much smaller area within the petrochemical complex. An analysis of high-resolution RGB imagery from Google Earth suggests that the plume originates from a flare stack. We estimated an emission rate of Q = 3.2 $\pm$ 0.9 t h^{-1}, which agrees with the one deduced from IASI with Q = 0.72 (0.36–4.28) t h^{-1}. A second plume was detected over another petrochemical complex in Iraq (top right). This plume also appears to originate from a flare stack, and an emission rate of Q = 3.7 $\pm$ 1.3 t h^{-1} was estimated. This region was not previously identified as an ethylene hotspot by Franco et al.,[3]. Possible explanations include differences in acquisition dates between the IASI observations and our measurements. The study of Franco et al.,[3] covered the period from 2008 to 2020, whereas the plume detected over Iraq was observed in 2023. Changes in industrial activity may therefore have occurred during this period.

In the bottom panels from Figure 2, we also show two acetylene plumes from other two sources. These sources are related to acetylene hotspots already detected by Franco et al.,[5] with IASI measurements. Both are located in China and are related to the petrochemical, coal, and metallurgy industry. Specifically, these two sources are related to facilities within industrial chemical complexes where acetylene is involved[30]. One of these emissions (bottom left) is located in the Wuhai region with a Q = 0.93 $\pm$ 0.16 t h^{-1}, while the other one (bottom right) is in the Bautou region with a Q = 3.2 $\pm$ 0.9 t h^{-1}. In the high-resolution image from Google Earth, we observe plumes of white smoke coming from nearby stacks and cooling towers in the Bautou emission. However, we checked the radiance reference band and discard the presence of this kind of plumes in this specific

source.

[Figure 2 about here.]

Additional visual inspection of the CH_4, CO_2, NH_3, and H_2O retrievals was carried out to assess whether the plumes shown in Figure 2 could be false positives. Part of this assessment is illustrated in Figure 3 and 4, where the ethylene and acetylene retrievals are compared to that of methane and ammonia, respectively. We select these gas retrievals since they are the main species that interfere with ethylene and acetylene absorption. Note that the analyzed sources are marked with red dots. We observe no correlation with other gases either, which increases confidence in the plumes.

[Figure 3 about here.]

[Figure 4 about here.]

Imaging spectrometers with characteristics similar to those used in this study, including the AVIRIS family[31], EnMAP[32], PRISMA[33], GF-5 AHSI[34], and Tanager-1[35], are promising candidates for ethylene and acetylene plume detection. Upcoming missions such as CHIME[36], as well as future Carbon Mapper instruments, are also expected to provide valuable capabilities for the plume detection and quantification of these gases.

Data and code availability

- Code for retrievals, plume delineation, and quantification is available at `https://github.com/jarojuan96/HS_tool`. The repository also contains lookup tables of radiance spectra for ethylene, acetylene, CH_4, CO_2, NH_3, and H_2O. Additional updates related to ethylene and acetylene retrievals have been implemented for this study relative to Roger et al.[15] and previous versions of this work.
- L1 data from EMIT are open to the public and is available through the Earthdata Search portal: `https://www.earthdata.nasa.gov/data/catalog/lpcloud-emitl1brad-001`

Acknowledgements

This research is partly funded by the Spanish Ministry of Science, Innovation and Universities (Grant PID2023-148485OB-C21/C22 funded by MCIU/AEI/10.13039/501100011033 ERDF, EU).

References

1. Atkinson, R. & Arey, J. Atmospheric degradation of volatile organic compounds. *Chemical Reviews* **103**, 4605–4638 (2003). URL https://doi.org/10.1021/cr0206420. PMID: 14664626, https://doi.org/10.1021/cr0206420.

2. Amghizar, I., Vandewalle, L. A., Van Geem, K. M. & Marin, G. B. New trends in olefin production. *Engineering* **3**, 171–178 (2017). URL https://www.sciencedirect.com/science/article/pii/S2095809917302965.

3. Franco, B. *et al.* Ethylene industrial emitters seen from space. *Nature Communications* **13**, 6452 (2022). URL https://doi.org/10.1038/s41467-022-34098-8.

4. Clerbaux, C. *et al.* The iasi/metop1 mission: First observations and highlights of its potential contribution to gmes2. *Space Research Today* **168**, 19–24 (2007). URL https://www.sciencedirect.com/science/article/pii/S0045873207800465.

5. Franco, B. *et al.* Satellite-based identification of large anthropogenic nmvoc emission sources. *Journal of Geophysical Research: Atmospheres* **129**, e2024JD042047 (2024). URL https://agupubs.onlinelibrary.wiley.com/doi/abs/10.1029/2024JD042047. E2024JD042047 2024JD042047, https://agupubs.onlinelibrary.wiley.com/doi/pdf/10.1029/2024JD042047.

6. Pässler, P. *et al.* *Acetylene* (John Wiley Sons, Ltd, 2011). URL https://onlinelibrary.wiley.com/doi/abs/10.1002/14356007.a01_097.pub4. https://onlinelibrary.wiley.com/doi/pdf/10.1002/14356007.a01_097.pub4.

7. Zhang, G. *et al.* Absorption spectroscopy of ethylene near 1.62 µm at high temperatures. *Journal of Quantitative Spectroscopy and Radiative Transfer* **241**, 106748 (2020). URL https://www.sciencedirect.com/science/article/pii/S0022407319306272.

8. Sharpe, S. W. *et al.* Gas-phase databases for quantitative infrared spectroscopy. *Applied Spectroscopy* **58**, 1452–1461 (2004).

9. Bertin, T. *et al.* The hitran2024 methane update. *Journal of Quantitative Spectroscopy and Radiative Transfer* **349**, 109736 (2026). URL https://www.sciencedirect.com/science/article/pii/S002240732500398X.

10. Connelly, D. S. *et al.* The emit mission information yield for mineral dust radiative forcing. *Remote Sensing of Environment* **258**, 112380 (2021). URL https://www.sciencedirect.com/science/article/pii/S0034425721000985.

11. Thorpe, A. K. *et al.* Attribution of individual methane and carbon dioxide emission sources using emit observations from space. *Science Advances* **9**, eadh2391 (2023). URL https://www.science.org/doi/abs/10.1126/sciadv.adh2391. https://www.science.org/doi/pdf/10.1126/sciadv.adh2391.

12. Roger, J., Guanter, L. & Gorroño, J. Assessing the detection of methane plumes in offshore areas using high-resolution imaging spectrometers. *Atmospheric Measurement Techniques* **18**, 5545–5567 (2025). URL https://amt.copernicus.org/articles/18/5545/2025/.

13. Růžička, V. *et al.* Fully automatic trace gas plume detection (2026). URL https://arxiv.org/abs/2605.03372. 2605.03372.

14. Thompson, D. R. *et al.* Space-based remote imaging spectroscopy of the aliso canyon ch4 superemitter. *Geophysical Research Letters* **43**, 6571–6578 (2016). URL https://agupubs.onlinelibrary.wiley.com/doi/abs/10.1002/2016GL069079. https://agupubs.onlinelibrary.wiley.com/doi/pdf/10.1002/2016GL069079.

15. Roger, J. *et al.* Remote sensing of ammonia point sources at high spatial resolution with satellite-based imaging spectrometers (2026). URL https://doi.org/10.31223/X5Q20M. Preprint.

16. Eriksson, P., Buehler, S., Davis, C., Emde, C. & Lemke, O. Arts, the atmospheric radiative transfer simulator, version 2. *Journal of Quantitative Spectroscopy and Radiative Transfer* **112**, 1551–1558 (2011). URL https://www.sciencedirect.com/science/article/pii/S0022407311001105.

17. Mayer, B. & Kylling, A. Technical note: The libradtran software package for radiative transfer calculations - description and examples of use. *Atmospheric Chemistry and Physics* **5**, 1855–1877 (2005). URL https://acp.copernicus.org/articles/5/1855/2005/.

18. Dudhia, A. The reference forward model (rfm). *Journal of Quantitative Spectroscopy and Radiative Transfer* **186**, 243–253 (2017). URL https://www.sciencedirect.com/science/article/pii/S0022407316301029. Satellite Remote Sensing and Spectroscopy: Joint ACE-Odin Meeting, October 2015.

19. Foote, M. D. *et al.* Impact of scene-specific enhancement spectra on matched filter greenhouse gas retrievals from imaging spectroscopy. *Remote Sensing of Environment* **264**, 112574 (2021). URL https://www.sciencedirect.com/science/article/pii/S0034425721002947.

20. Coheur, P.-F., Clarisse, L., Turquety, S., Hurtmans, D. & Clerbaux, C. Iasi measurements of reactive trace species in biomass burning plumes. *Atmospheric Chemistry and Physics* **9**, 5655–5667 (2009). URL https://acp.copernicus.org/articles/9/5655/2009/.

21. Logan, J. A., Prather, M. J., Wofsy, S. C. & McElroy, M. B. Tropospheric chemistry: A global perspective. *Journal of Geophysical Research: Oceans* **86**, 7210–7254 (1981). URL https://agupubs.onlinelibrary.wiley.com/doi/abs/10.1029/JC086iC08p07210. https://agupubs.onlinelibrary.wiley.com/doi/pdf/10.1029/JC086iC08p07210.

22. Kochanov, R. *et al.* Hitran application programming interface (hapi): A comprehensive approach to working with spectroscopic data. *Journal of Quantitative Spectroscopy and Radiative Transfer* **177**, 15–30 (2016). URL https://www.sciencedirect.com/science/article/pii/S0022407315302466. XVIIIth Symposium on High Resolution Molecular Spectroscopy (HighRus-2015), Tomsk, Russia.

23. Frankenberg, C. *et al.* Airborne methane remote measurements reveal heavy-tail flux distribution in four corners region. *Proceedings of the National Academy of Sciences* **113**, 9734–9739 (2016). URL https://www.pnas.org/doi/abs/10.1073/pnas.1605617113. https://www.pnas.org/doi/pdf/10.1073/pnas.1605617113.

24. Varon, D. J. *et al.* Quantifying methane point sources from fine-scale satellite observations of atmospheric methane plumes. *Atmospheric Measurement Techniques* **11**, 5673–5686 (2018). URL https://amt.copernicus.org/articles/11/5673/2018/.

25. Guanter, L. *et al.* Multisatellite data depicts a record-breaking methane leak from a well blowout. *Environmental Science & Technology Letters* **11**, 825–830 (2024). URL https://doi.org/10.1021/acs.estlett.4c00399. https://doi.org/10.1021/acs.estlett.4c00399.

26. Gorroño, J., Pei, Z., Valverde, A. & Guanter, L. Considering the observation and illumination angular configuration for an improved detection and quantification of methane emissions. *Atmospheric Measurement Techniques* **19**, 1245–1257 (2026). URL https://amt.copernicus.org/articles/19/1245/2026/.

27. Gorroño, J., Pei, Z. & Guanter, L. Benchmark simulations for methane emissions validation and sensitivity studies (2026). URL https://doi.org/10.5281/zenodo.18161182.

28. Molod, A. *et al.* The geos-5 atmospheric general circulation model: Mean climate and development from merra to fortuna. https://portal.nccs.nasa.gov/datashare/gmao/geos-fp/das/ (2012). Accessed: 12 June 2026.

29. Roger, J. *et al.* High-resolution methane mapping with the enmap satellite imaging spectroscopy mission. *IEEE Transactions on Geoscience and Remote Sensing* **62**, 1–12 (2024).

30. Baidu baike. https://baike.baidu.com/. Online encyclopedia, accessed: 2026-07-06.

31. Green, R. O. *et al.* Imaging spectroscopy and the airborne visible/infrared imaging spectrometer (aviris). *Remote Sensing of Environment* **65**, 227–248 (1998). URL https://www.sciencedirect.com/science/article/pii/S0034425798000649.

32. Guanter, L. *et al.* The enmap spaceborne imaging spectroscopy mission for earth observation. *Remote Sensing* **7**, 8830–8857 (2015). URL https://www.mdpi.com/2072-4292/7/7/8830.

33. Loizzo, R. *et al.* Prisma: The italian hyperspectral mission. In *IGARSS 2018 - 2018 IEEE International Geoscience and Remote Sensing Symposium*, 175–178 (2018).

34. Liu, Y.-N. *et al.* The advanced hyperspectral imager: Aboard china's gaofen-5 satellite. *IEEE Geoscience and Remote Sensing Magazine* **7**, 23–32 (2019).

35. Duren, R. *et al.* The carbon mapper emissions monitoring system. *Atmospheric Measurement Techniques* **18**, 6933–6958 (2025). URL https://amt.copernicus.org/articles/18/6933/2025/.

36. Celesti, M. *et al.* The copernicus hyperspectral imaging mission for the environment (chime): Status and planning. In *IGARSS 2022 - 2022 IEEE International Geoscience and Remote Sensing Symposium*, 5011–5014 (2022).

Competing interests: The authors declare no competing interests.

List of Figures

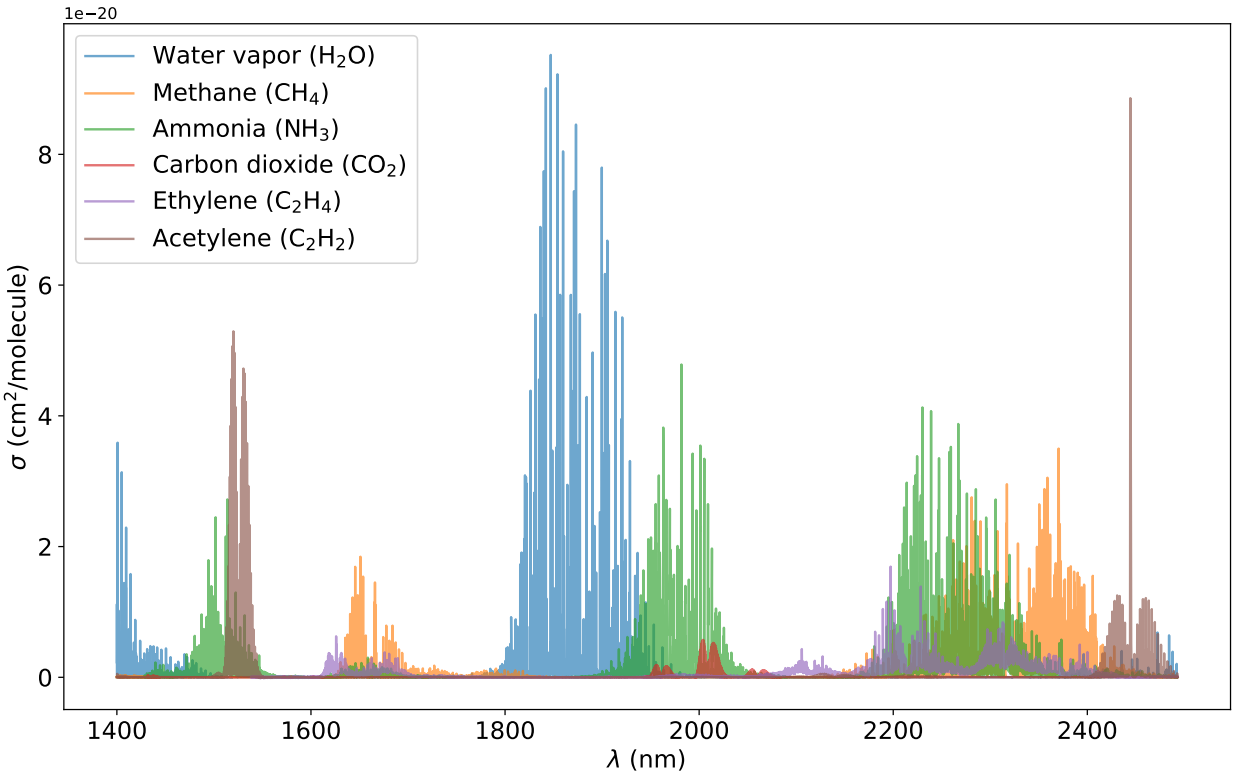

Figure 1: High-resolution cross section spectra of water vapor (blue), methane (orange), ammonia (green), carbon dioxide (red), ethylene (purple), and acetylene (brown). All these spectra were obtained for pressure and temperature conditions of P = 1 atm and T = 294 K, respectively, except for ethylene with P = 1 atm and T = 298.1 K.

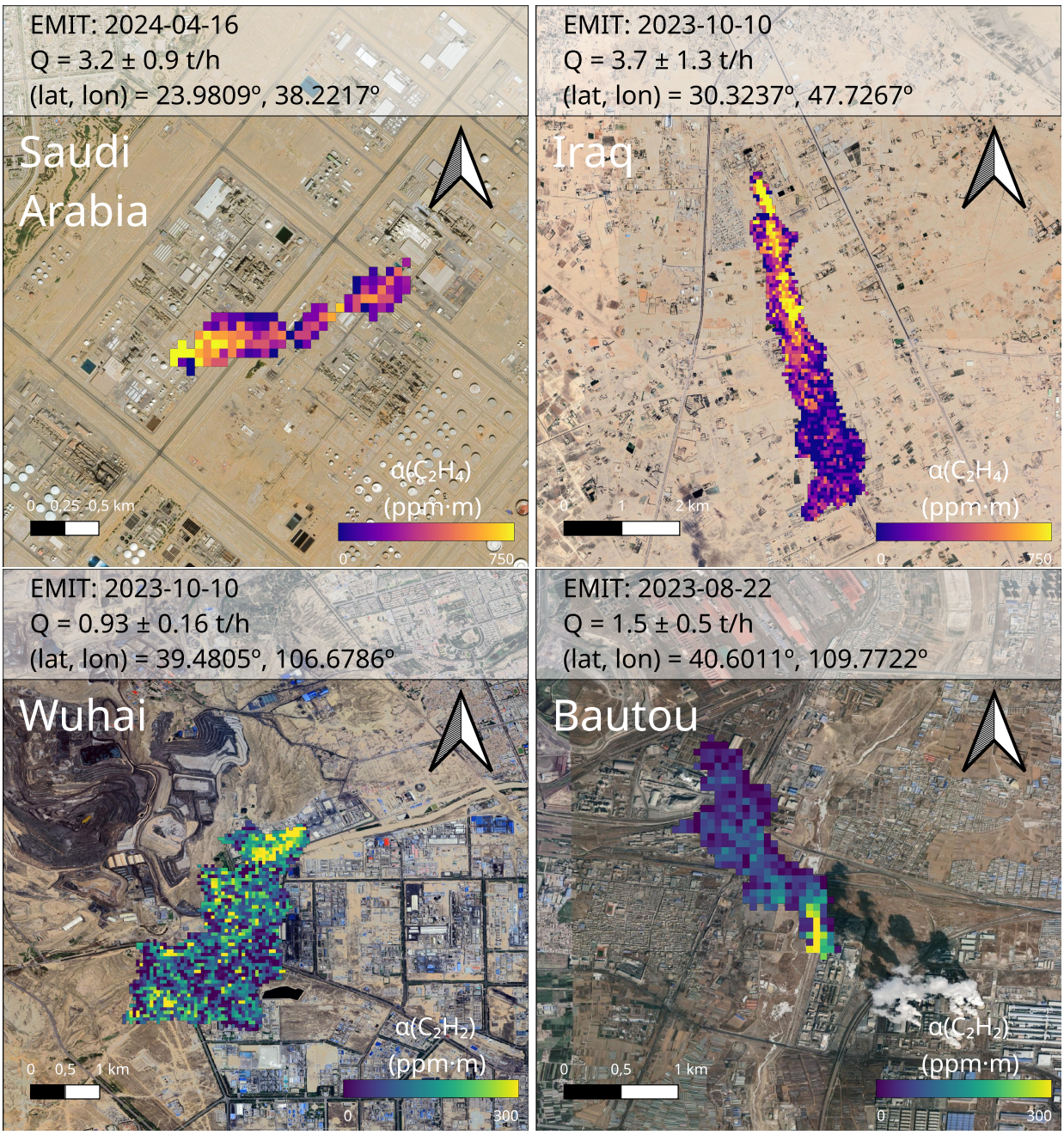

Figure 2: Examples of two ethylene (top panels) and acetylene plumes (bottom panels) overlaid on high-resolution Google Earth images (© Google Earth; data provider: Airbus and Maxar Technologies). All these plumes were characterized using EMIT data and were originated from industrial sources. Details of the ethylene concentration-path length enhancement levels, location, acquisition date, source coordinates, and emission quantification can be found for each plume.

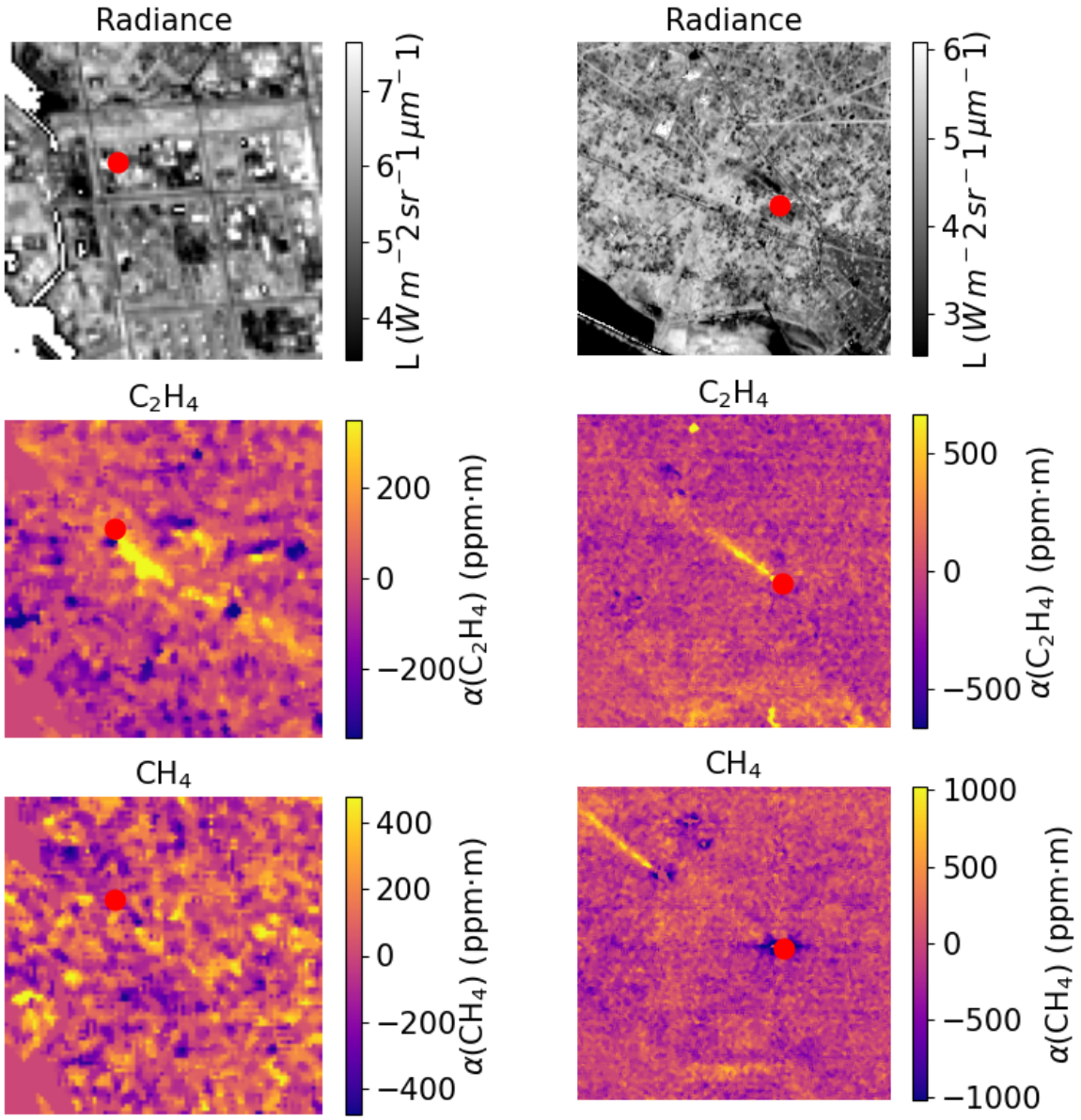

Figure 3: Analysis of potential ethylene emission correlation with methane retrievals for the Saudi Arabia (Figure 2: top-left) and Iraq (Figure 2: top-right) plumes. Starting from the top: radiance reference band, ethylene, and CH_4 retrievals. The ethylene sources are marked with a red dot in all the panels. Note that the plume orientation differs from that shown in Figure 2, where the retrievals are georeferenced.

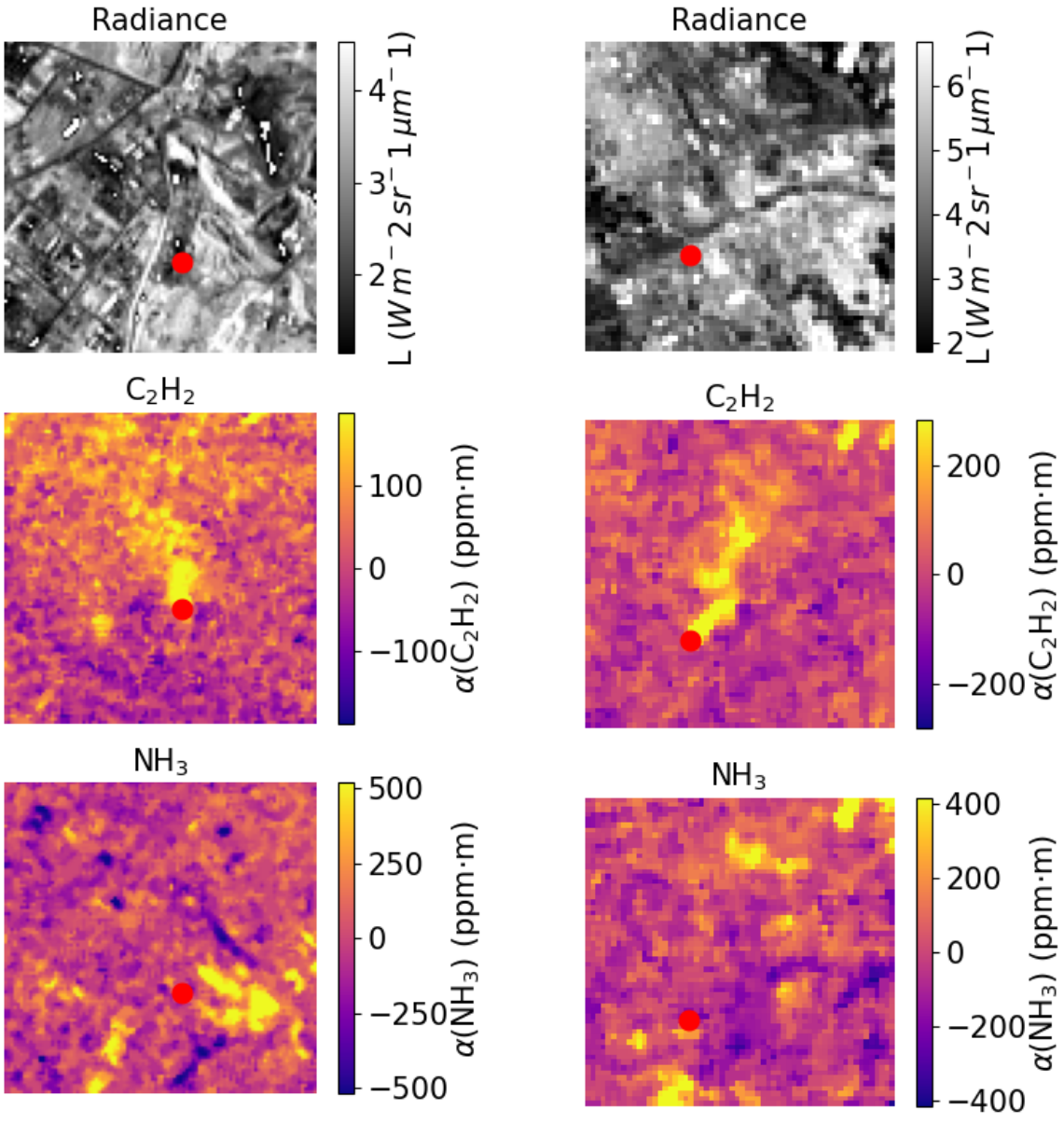

Figure 4: Analysis of potential acetylene emission correlation with ammonia retrievals for the Wuhai (Figure 2: bottom-left) and Wuhai (Figure 2: bottom-right) plumes. Starting from the top: radiance reference band, acetylene, and NH_3 retrievals. The acetylene sources are marked with a red dot in all the panels. Note that the plume orientation differs from that shown in Figure 2, where the retrievals are georeferenced.